Composites Science and Technology 238 (2023) 110048

Contents lists available at ScienceDirect

Composites Science and Technology

journal homepage: www.elsevier.com/locate/compscitech

Fabrication of carbon fiber/polyamide 6 composites with water resistance and anti-icing performance using a superhydrophobic fluorinated-polydopamine coating

Seung Mo Son [a,1], Minjung Kim [b,1], Jung Jae Yoo [a], Min Seong Kim [b], Byeong-Su Kim [b,**], Dong Gi Seong [a,c,*]

[a] School of Chemical Engineering, Pusan National University, Busandaehak-ro 63beon-gil 2, Geumjeong-gu, Busan, 46241, Republic of Korea
[b] Department of Chemistry, Yonsei University, Seoul, 03722, Republic of Korea
[c] Department of Polymer Science and Engineering, Pusan National University, Busandaehak-ro 63beon-gil 2, Geumjeong-gu, Busan, 46241, Republic of Korea

ARTICLE INFO

Handling Editor: Ming-Qiu Zhang

Keywords:
A. Carbon fibres
A. Multifunctional composites
B. Multifunctional properties
B. Surface treatments
E. Resin transfer moulding (RTM)

ABSTRACT

With the advance of the reactive liquid molding process for mass production, polyamide 6 (PA 6)-based carbon fiber reinforced thermoplastic (CFRTP) with excellent impact resistance and recyclability has been developed, but there is still a limit to the application of external parts due to deterioration of mechanical properties in a moisture environment. This study proposes an efficient process that is advantageous for the mass production of CFRTP with improved water stability by coating fluorinated polydopamine (*f*-PDA) on PA 6-based CFRTP fabricated by the thermoplastic resin transfer molding process. Compared to neat CFRTP, the interlaminar shear strength and flexural strength of the CFRTP immersed in water improved by 16% and 31%, respectively, with a significant reduction in water absorption of 42%. Furthermore, the anti-icing performance of the CFRTP was verified, as evidenced by a 49% reduction in surface energy. The proposed *f*-PDA-CFRTP is anticipated to be applied to external parts in various transportation industries while ensuring environmental reliability.

1. Introduction

The global demand for lightweight materials is rapidly increasing to improve the fuel efficiency of mobility and to reduce the emissions of greenhouse gases and carbon cycle decomposition. Carbon fiber reinforced thermoplastic (CFRTP) stands out as a representative lightweight material because of its superior mechanical properties [1]. Polyamide 6 (PA 6)-based CFRTP, in particular, has superior impact resistance because of its impact absorption effect in an amorphous region and is thus regarded as a sustainable structural material owing to its recyclability [[2–4]]. For the mass production of PA 6-based CFRTP, thermoplastic resin transfer molding (T-RTM) is one of the promising processes. T-RTM process has excellent processability because it uses ε-caprolactam as an injected monomer with a significantly lower viscosity than the molten polymer [[5–10]].

Although PA 6-based CFRTP has excellent mechanical properties, its intrinsic hydrophilicity often leads to the absorption of water, which interrupts the intermolecular hydrogen bonding of PA 6 as a plasticizer in the amorphous region of the matrix, thus degrading the properties of the polymer [11]. Additionally, water penetrates matrix and carbon fiber interface, which causes deterioration of the mechanical properties of the entire CFRTP [12,13].

Furthermore, PA 6 has a disadvantage in which undesirable materials adhere to the surface due to its high surface energy [14]. Vessels face the problem of increasing wave resistance and fuel consumption due to marine life on the water surface [15,16]. The icing on the surface of aircraft causes failure and accidents, which takes time and costs to de-ice [17]. Wind power generators have a problem of reducing power generation by 30% and poor reliability due to icing [18]. To ensure the environmental reliability of a final product, it is therefore essential to reduce surface energy prior to applying PA 6-based CFRTP as an external component [19].

* Corresponding author. School of Chemical Engineering, Pusan National University, Busandaehak-ro 63beon-gil 2, Geumjeong-gu, Busan, 46241, Republic of Korea.
** Corresponding author.
E-mail addresses: bskim19@yonsei.ac.kr (B.-S. Kim), dgseong@pusan.ac.kr (D.G. Seong).
[1] These authors contributed equally to this work.

https://doi.org/10.1016/j.compscitech.2023.110048
Received 5 January 2023; Received in revised form 14 April 2023; Accepted 18 April 2023
Available online 18 April 2023

Attempts have been made to overcome these critical challenges by irradiating the surface with a laser to modify matrix and by replacing the surface functional group with fluorine [20]. However, this method is unsuitable for coating large products such as ships, aircraft, wind power generators, and other curved products. Numerous modifications have been made to modify the surface to alleviate the aforementioned challenges; however, all have some limitations in performance or processability. For example, poly(vinylidene fluoride) (PVDF), a fluorine-based polymer, can be used as a CFRTP matrix because of its excellent waterproof performance [21]. However, due to low surface energy in the matrix, the interfacial bonding between the fiber and matrix is weak, and the tensile strength of the composite is about 100 MPa, which is insufficient to be used for structural components. Additionally, the impregnation of PVDF melt with high viscosity into the fabric is difficult and time-consuming, which is disadvantageous to the mass production of large-sized products.

In this context, this study uses the T-RTM process to fabricate a PA 6-based CFRTP and introduces a highly adhesive and hydrophobic layer on the surface of the composite to overcome the limitations in mass-processability and water-based degradation of physical properties. By taking advantages of the versatile surface coating nature irrespective of the type of substrates, a mussel-inspired polydopamine (PDA) was employed for surface modification [[22–25]]. Specifically, PDA is initially polymerized on the surface of CFRTP and subsequently modified with fluorinated molecules via a Michael-type addition reaction to achieve antifouling performance and stability against water in CFRTP [26,27]. Fig. 1 shows the overall T-RTM process and the surface modification procedures used. Through the *f*-PDA coating, it is possible to improve the mechanical properties of CFRTP and exhibit superior surface performances. Eventually, low surface energy and wettability are introduced into CFRTP with *f*-PDA coating to overcome the problems that occur when applied as external components. Since the relatively simple dip-coating method is used, it is more efficient for the surface treatment of large and curved products. PDA-based surface modification is a reliable and robust coating method to fluorinate most kinds of nanoparticles or substrates with strong adhesive force by covalent and noncovalent interactions [28]. In addition, PDA can be applied to the spray coating process, it will be advantageous to expand this protocol to the coating of large, curved, and complex-shaped products [29,30]. Structural characterizations are performed to prove the successful coating of *f*-PDA on the surface of CFRTP. The mechanical properties after immersion in water are measured to investigate the improvement of water resistance along with the related structural analyses, including the surface morphology and energy. Moreover, the anti-icing test of the resultant CFRTP is conducted to show the applicability to wide ranges of mobility, such as vehicles, ships, and aircraft.

2. Experimental

2.1. Materials

ε-Caprolactam (Sigma-Aldrich), *N*-acetylcaprolactam (Sigma-Aldrich), and ethylmagnesiumbromide (Sigma-Aldrich) were used as monomers, activators, and catalysts, respectively. 12 K Plain weave WSN 3KY (Hyundai Fiber co. Ltd, Korea) was used as a carbon fiber reinforcement material. Dopamine hydrochloride (Sigma-Aldrich), 1H,1H,2H,2H-perfluorodecanethiol (Sigma-Aldrich), 2,2,3,3,4,4,4-Heptafluorobutylamine (Alfa-Aeear), 1,4-dioxane (SAMCHUN), 1 M Tris-

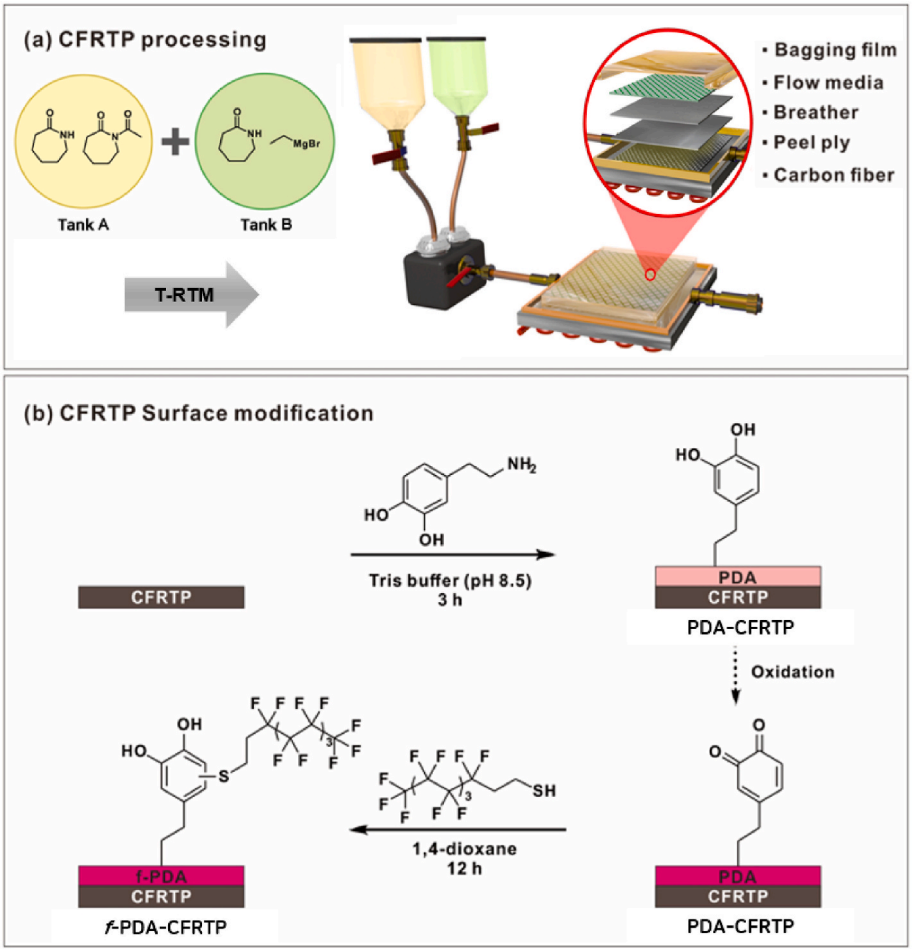

Fig. 1. (a) Scheme of the overall T-RTM process and (b) the surface modification procedures to yield PDA-CFRTP and *f*-PDA-CFRTP.

HCl (pH 8.5) (Tech&Innovation (T&I)) were used as coating agents. Diiodomethane (Sigma-Aldrich) was used to measure the contact angle. All chemicals were of analytical reagent grade and were used without purification unless otherwise indicated.

2.2. Preparation of PA 6-based CFRTP

The carbon fiber was dried in a vacuum oven at 80 °C for 48 h and then placed in the mold. After that, peel ply, breather, flow media, and bagging film were sequentially laminated on the carbon fiber to impregnate the entire fiber. In preparation for resin, ε-caprolactam was dissolved in a nitrogen atmosphere at 75 °C and a catalyst was injected. Then, stirring and degassing were performed at 75 °C for 30 min to remove residual moisture. After the degassing process, the initiator was injected into the resin and stirred for 1 min. Subsequently, the resin was impregnated into the carbon fiber located in the mold using a vacuum pump and polymerized at 150 °C for 1 h to complete the final T-RTM process. Finally, the mold was cooled at room temperature for 1 h, and then CFRTP was obtained. The average fiber volume fraction of the CFRTP was 52%. In this study, plate-shaped CFRTP was cut according to the test specimen size, unlike real CFRTP parts in the industry which are fully immersed in the dip coating process by *f*-PDA on the top, bottom, and lateral sides. This cutting process exposed carbon fibers on the cutting sides, leading to undesirable water penetration and deterioration of mechanical properties. To exclude this effect, we coated the sidewall with Al spray to prevent water penetration and investigated the effect of *f*-PDA coating only on the top and bottom sides.

2.3. Surface modification

2.3.1. Modification of polydopamine (PDA)

The synthesis of PDA was prepared by referring to the experimental procedures of Lee et al. with slight modifications [22]. First, 1.0-M Tris buffer (pH 8.5) was mixed with deionized (DI) water to obtain the desired solution. Subsequently, dopamine hydrochloride (400 mg) was dissolved in 10-mM Tris buffer (pH 8.5, 40 mL). The color of the mixed solution became dark brown within minutes. Immediately, prepared substrates were immersed vertically in a 10 mg/mL dopamine solution with stirring. After coating for 3 h, PDA-coated substrates were thoroughly washed with water and dried with N_2 gas. Subsequently, the solvent in the substrates was completely dried under vacuum at 80 °C before additional treatment.

2.3.2. Post-modification of fluorine (f-PDA)

1H,1H,2H,2H-perfluorodecanethiol (400 mg) was dissolved in 40 mL of 1,4-dioxane. As described above, PDA-coated substrates were immersed vertically into a 10 mg/mL fluorine solution with stirring. After 12 h, *f*-PDA-coated substrates were washed with 1,4-dioxane and dried with N_2 gas. Subsequently, to remove the remaining solvent completely, *f*-PDA-coated substrates were dried under a vacuum at 80 °C. The prepared samples were stored under a vacuum at 25 °C prior to mechanical analysis.

2.4. Analysis methods

The surface morphology of the specimens was analyzed by using atomic force microscopy (AFM, Icon-PT-PLUS). In a tapping mode, a 50 μm × 50 μm section was scanned at 0.8 Hz. Chemical states were analyzed using a *K*-alpha X-ray photoelectron spectroscopy (XPS, Thermo-Fisher, USA). Scanning electron microscopy (SEM) measurements were conducted using the IT-500HR (JEOL) instrument at an accelerating voltage of 10 kV. Energy-dispersive X-ray spectroscopy (EDS) coupled with SEM was employed at an accelerating voltage of 15 kV.

The thickness of the samples on the silicon substrates was obtained using ellipsometry (J. A. Woollam Co. Inc., EC-400 and M-2000 V). The static contact angles of water on the coated substrates were measured to analyze the surface modification. Prior to use, the SiO_2 substrate was cleaned and then incubated for 3 and 12 h in 10 mg/mL polymer solutions in Tris buffer and 1,4-dioxane, respectively, at room temperature. After incubation, the substrate was washed five times with each solvent and dried with nitrogen. All samples were analyzed at least five times, and the average value was reported with the standard deviation as the error range.

A contact angle goniometer (Phoenix 300) was used to analyze changes in the hydrophilicity of CFRTP by measuring static contact angles. The chemical stability of *f*-PDA-CFRTP was evaluated by measuring the static contact angles of aqueous HCl and NaOH solutions at pH 1 to 13. The thermal stability of *f*-PDA-CFRTP was assessed by measuring the static contact angle after exposure to temperatures ranging from −30 °C to 210 °C for 30 min at each temperature. To investigate the wear resistance of *f*-PDA-CFRTP, an abrasion test was conducted using 800 grit sandpaper and a 400 g weight, with an abrasion cycle involving a 6 cm movement at 20 mm/s. The static contact angle was measured before and after the abrasion test. The drop volume was about 10 μL, the relative humidity was 40%, and water and diiodomethane were used for measurement. The average value was determined by measuring each specimen nine times. The water absorption was measured by immersing the CFRTP in distilled water at 60 °C and measuring the mass change. The water absorption of CFRTP was calculated using the following equation.

$$Water\ absorption\ (\%) = \frac{W_{wet} - W_{dry}}{W_{dry}} \text{ x } 100 \quad (1)$$

where w_{wet} and w_{dry} are the weights of the wet and dry samples, respectively.

Three hundred-magnification cross-sectional images of the specimens were taken using an optical microscope (Nikon Eclipse LV100ND). The void contents of the dry and water absorbed specimens were quantified using the contrast ratio with the Image J program. At least 15 sections per specimen were analyzed to measure the average void contents. A universal testing machine (UTM, RB 301 UNITECH, R&B) was used to measure the mechanical properties of CFRTP.

Interlaminar shear strength (ILSS) was measured according to ASTM D2344, and flexural strength was measured according to ASTM D790. The mechanical properties of the dried specimens were measured after drying in a vacuum oven at 80 °C for 48 h, and the mechanical properties of the wet specimens were measured after immersion in distilled water at 60 °C for 9 h. A double-channel microsyringe pump (PHD 2000 Infusion, Harvard apparatus) was used to perform the anti-icing test [20]. After conditioning the 60 × 25 mm specimens in a cryogenic freezer (WSN-5700UC, Woosung) at −10 °C for 30 min, 0 °C water was continuously dropped onto the specimen and the flow behavior was observed. The drop speed was 2 mL/min, and the slope of the specimen was set to 45°. The distance between the specimen and the nozzle was 10 cm.

3. Results and discussion

3.1. Surface coating

Dopamine coating conditions were optimized on a silicon wafer as the model substrate before being applied to CFRTP. The silicon wafer substrate was coated in a solution of dopamine hydrochloride in Tris buffer using a dipping method. It was observed that the color of the silicon wafer became dark blue, indicating that the coating successfully proceeded through the oxidation and self-polymerization of dopamine (Fig. S1). The thickness of the PDA-coated surfaces was investigated using ellipsometry (Fig. S2). The surface thicknesses of the PDA-coated silicon wafers (i.e., PDA-SiO_2) in different concentrations of dopamine solution for 3 h were measured to be 17.3 and 38.1 nm for 2.0 and 10

mg/mL, respectively. Increasing coating time from 3 to 12 h at 2.0 mg/mL increased the surface coating thickness to the same thickness as in 10 mg/mL. Considering the vulnerable nature of CFRTP in water, the coating time was limited to minimize the possible exposure to water. Subsequently, 1H,1H,2H,2H-perfluorodecanethiol was coated on a prepared PDA-SiO_2 substrate in the same manner described above to afford the fluorinated surface coating (i.e., *f*-PDA-SiO_2). The fluorine coating was optimized to produce the coated substrates with sufficient hydrophobicity of a higher contact angle.

The static contact angles of water on the coated substrates were measured to analyze the surface modification. While the bare silicon wafer showed a static contact angle of 65.2°, the PDA-SiO_2 substrate showed a reduced contact angle of 47.2°, suggesting a relative hydrophilic coating on the surface with PDA. However, this reduced contact angle increased sharply upon treatment with fluorinated molecules to yield *f*-PDA-SiO_2 displaying a more increased contact angle of 80.3°, indicating the successful formation of a hydrophobic surface.

Additionally, XPS was used to verify the chemical composition of each substrate (Fig. 2). PDA-SiO_2 mainly consisted of carbon (71.8 at.%), oxygen (20.2 at.%), and nitrogen peak (7.3 at.%). Upon coating with perfluorodecanethiol on the PDA surfaces, the atomic composition of *f*-PDA-SiO_2 surfaces consisted of carbon (67.4 at.%) and oxygen (20.6 at.%), nitrogen peak (6.5%) and fluorine peak (4.9 at.%), clearly indicating the successful introduction of fluorine coating.

3.2. Surface analysis

The surface morphology changes of CFRTP upon coating with PDA and *f*-PDA were further analyzed using AFM (Fig. 3, and Fig. S3). The overall height of the CFRTP was constant in the height-mode image, and some fine roughness was observed on the surface when the CFRTP was demolded. However, in the case of PDA-CFRTP and *f*-PDA-CFRTP, the formation of roughness within 1 μm was observed. This is because PDA generally forms spherical aggregates when polymerized [22], and its shape is maintained even when a functional group is modified with fluorine.

CFRTP showed a linear woven structure of carbon fibers on the surface. However, this was not observed in PDA-CFRTP and *f*-PDA-CFRTP, indicating that PDA was coated uniformly on the entire surface. The 3D image of each specimen confirmed that the PDA and *f*-PDA-coated specimens had a roughness within 1 μm. CFRTP had a root-mean-squared roughness (R_{RMS}) value of 71.9 nm. However, PDA-CFRTP had an R_{RMS} value of 127 nm caused by aggregation, and *f*-PDA-CFRTP had a value of 132 nm similar to that of PDA. Analyzing a large area of the 50 × 50-μm section using AFM verified that PDA was well polymerized on the CFRTP surface.

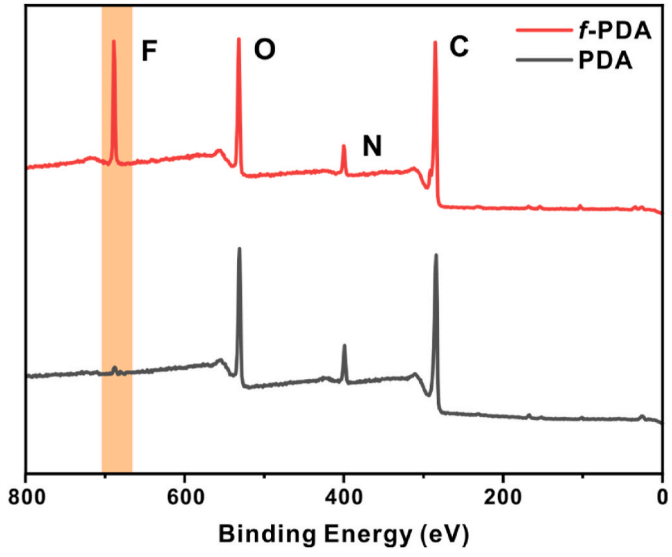

Fig. 2. XPS spectra for PDA (black) and *f*-PDA-coated (red) silicon wafer substrate.

Similar to AFM analysis, SEM was used to observe changes in the morphology of CFRTP after each surface modification (Fig. 4). No aggregation was observed on the surface of CFRTP, whereas the spherical particles with a diameter of about 200 nm were observed in large areas in PDA-CFRTP and *f*-PDA-CFRTP. As previously stated, it was confirmed that this was a typical PDA aggregation shape and the PDA was well coated on the surface. Additionally, since the shape of *f*-PDA-CFRTP is similar to that of PDA-CFRTP, it was confirmed that fluorinating the PDA surface did not affect its morphology, confirming a non-destructive nature of the surface coating. Furthermore, PDA covered fine surface voids formed by incomplete impregnation of the resin, thus preventing water diffusion into the surface voids upon exposure to water. Combining these findings, it was found that the PDA coating improves the hydrophobic performance by filling defects like voids and fiber weaving patterns and creating nanometer-level roughness to change the surface to the Cassie–Baxter state [[31–34]]. Furthermore, the EDS mapping suggested the successful surface modification of each coating in good agreement with XPS analysis (Fig. S4, Table S1, Table S2).

3.3. Water resistance and durability tests

The static contact angle was measured to confirm the hydrophilicity and hydrophobicity of the coated specimen (Fig. 5). The pristine CFRTP had the lowest contact angle of 64.4°. Upon coating with PDA, the contact angle of PDA-CFRTP was slightly increased to 74.2°, indicating a relatively more hydrophobic nature of PDA coating. Furthermore, the contact angle of *f*-PDA-CFRTP increased considerably to 93.2°, which indicated the most hydrophobic nature among all three surfaces. On the basis of the AFM and SEM results, the hydrophobic surface in the Cassie–Baxter state repels water because *f*-PDA-CFRTP has a larger surface area caused by aggregation [31,32]. The chemical, thermal, and wear resistances of *f*-PDA-CFRTP were also evaluated. The static contact angles of *f*-PDA-CFRTP did not decrease after exposure to aqueous HCl and NaOH solutions of various pH ranges. Additionally, the *f*-PDA coating remained intact after temperature exposure tests ranging from −30 °C to 210 °C and a sandpaper wear test of 200 cycles. These results indicate that *f*-PDA-CFRTP exhibits good chemical, thermal, and wear resistances, further confirming its potential for wider industrial applications.

To confirm the effect of preventing the deterioration of properties of PA 6 due to water absorption, specimens were immersed in 60 °C water for 30 days. Fig. 6 shows the water absorption behavior of CFRTP, PDA-CFRTP, and *f*-PDA-CFRTP. CFRTP absorbed water most rapidly in the water absorption test. Water penetrates the amorphous region of the PA 6 and the interface between the carbon fiber and the matrix because CFRTP has the most hydrophilic surface [12]. Additionally, there are three possible reasons for unstable behavior in the early stages of water absorption of CFRTP: i) the presence of unreacted residual *ε*-caprolactam due to an incomplete degree of conversion; ii) the hydrolysis of PA 6 under hot water; iii) re-crystallization of the amorphous region of PA 6 at high temperature that can release the absorbed water [[11, 12, [35,36]].

In stark contrast to the aforementioned postulation, all coated composites of PDA-CFRTP and *f*-PDA-CFRTP displayed significantly lower water absorption, as shown in Fig. 6. This observation is due to the barrier effect of the PDA, which has a less hydrophilic surface than PA 6 and is consistent with the contact angle test. In addition to the barrier effect of the PDA, the fluorinated coating of *f*-PDA-CFRTP further prevented water absorption due to its high hydrophobicity. However, the water adsorption becomes similar to that of PDA-CFRTP after prolonged exposure in water 7 days. While *f*-PDA-CFRTP has low wettability, the water eventually penetrates the surface when exposed to harsh

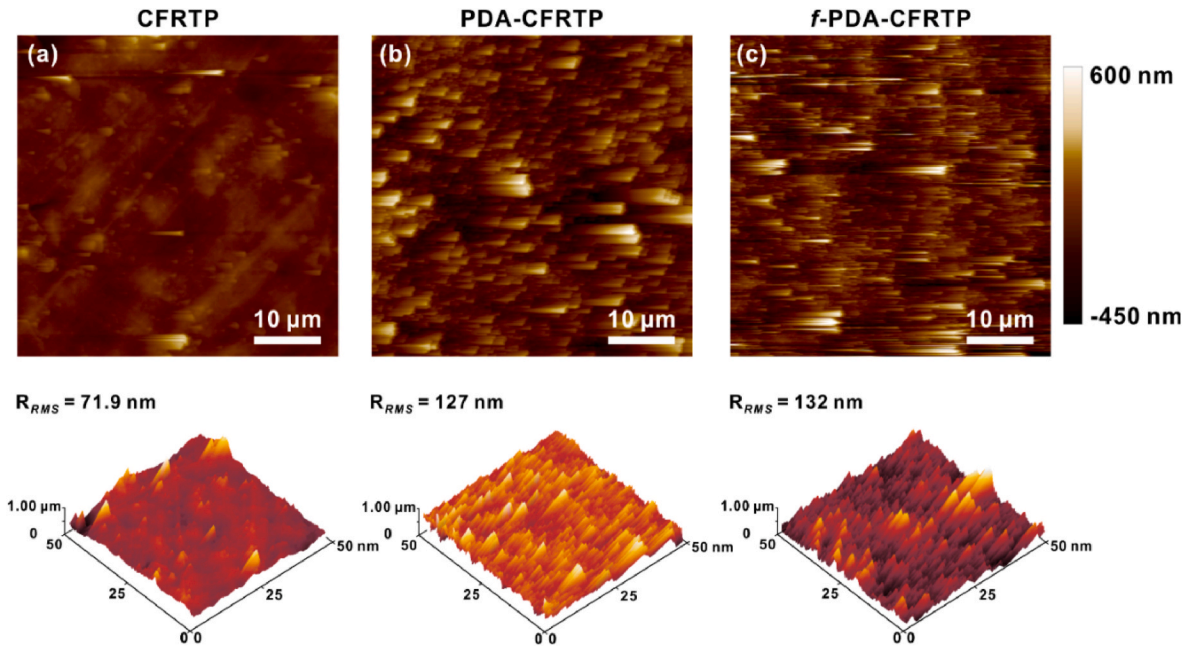

Fig. 3. Height-mode AFM images of (a) CFRTP, (b) PDA-CFRTP, and (c) *f*-PDA-CFRTP with the corresponding 3D perspective view and roughness values.

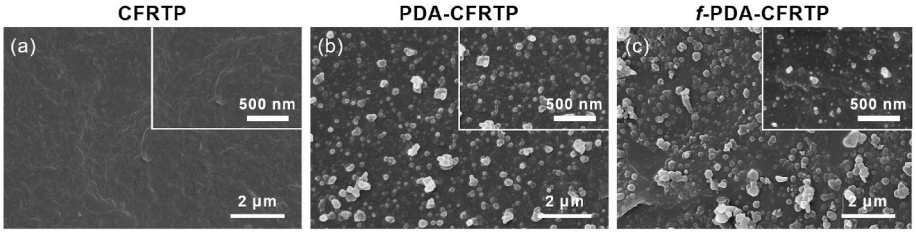

Fig. 4. SEM images of (a) CFRTP, (b) PDA-CFRTP, and (c) *f*-PDA-CFRTP with corresponding high-magnification in inset.

conditions for a long time. Nevertheless, the water absorption was 42% lower than that of CFRTP, indicating that the fluorinated PDA coating on CFRTP effectively prevents water penetration.

Based on Fick's law of diffusion, the water absorption of the composite was calculated to determine the diffusion coefficient of water (D_{water}) using the following equation [12].

$$D_{water} = \pi\left(\frac{h}{4M_m}\right)^2\left(\frac{M_2 - M_1}{\sqrt{t_2} - \sqrt{t_1}}\right)^2, \quad (2)$$

where h is the thickness of the specimen, M_m is the final water absorption mass, t_1 and t_2 are the arbitrary times in the linear section, and M_1 and M_2 are the water absorption masses at times t_1 and t_2, respectively. As a result of calculations based on the initial 12 h, the diffusion coefficients of CFRTP, PDA-CFRTP, and *f*-PDA-CFRTP gradually decreased to 139×10^{-7}, 89.2×10^{-7}, and 25.8×10^{-7} mm^2/s, respectively. Cross sections of the specimens were observed using optical microscopy to confirm the suppression of the hydrolysis of PA 6 due to coating. After 30 days of water absorption, CFRTP became hydrolyzed more than other coated specimens, and the void content reached 10.97% (Fig. S5). In comparison, the hydrolysis rates of PDA-CFRTP and *f*-PDA-CFRTP were considerably lower, resulting in relatively low void contents of 6.77% and 4.77%, respectively.

The ILSS test was conducted to investigate the change in interfacial bonding between the fiber and the composite material matrix due to water immersion (Fig. 7) [5]. The ILSS of dried CFRTP, PDA-CFRTP, and *f*-PDA-CFRTP were 65.7, 72.8, and 69.0 MPa, respectively, showing similar mechanical properties. This implies that the coating process does not deteriorate the ILSS of the composite material. The mechanical properties of immersed CFRTP and PDA-CFRTP were similarly reduced to 47.7 and 46.7 MPa, respectively. This is because water interrupts the hydrogen bond of PA 6, and the interfacial bonding force between the fiber and the matrix weakens. Despite the barrier effect, the immersed PDA-CFRTP has similar mechanical properties to CFRTP possibly due to the exposure to water during the PDA coating process. However, since *f*-PDA-CFRTP displayed the least water absorption, it showed a 16.2% improvement in ILSS of 56.8 MPa compared to CFRTP. The ILSS test proved the effectiveness of the *f*-PDA coating in enhancing mechanical properties even in a humid environment.

The flexural test was conducted to check the effect of water on the mechanical properties of the entire CFRTP and to verify the improvement effect of the coating (Fig. 7). The flexural strengths of dried CFRTP, PDA-CFRTP, and *f*-PDA-CFRTP were 779.4, 739.9, and 823.1 MPa, respectively, showing similar levels. However, immersed CFRTP, PDA-CFRTP, and *f*-PDA-CFRTP had flexural strengths of 346.0, 439.6, and 501.9 MPa, respectively, showing significant differences between specimens depending on the presence of coating. This is because the flexural strength reflects the deterioration of the mechanical properties of the entire specimen owing to water, whereas ILSS mainly reflects the properties of the interface. The flexural strengths of PDA-CFRTP and *f*-PDA-CFRTP were improved by 21.3% and 31.1%, respectively, compared to that of CFRTP, and thus the effectiveness of the waterproof performance of each coating was confirmed. Additionally, the flexural strength showed a greater change in water absorption than that of ILSS. Water penetrates the amorphous region of PA 6 and the interface of the carbon fiber and PA 6 by half. ILSS is mainly affected by water

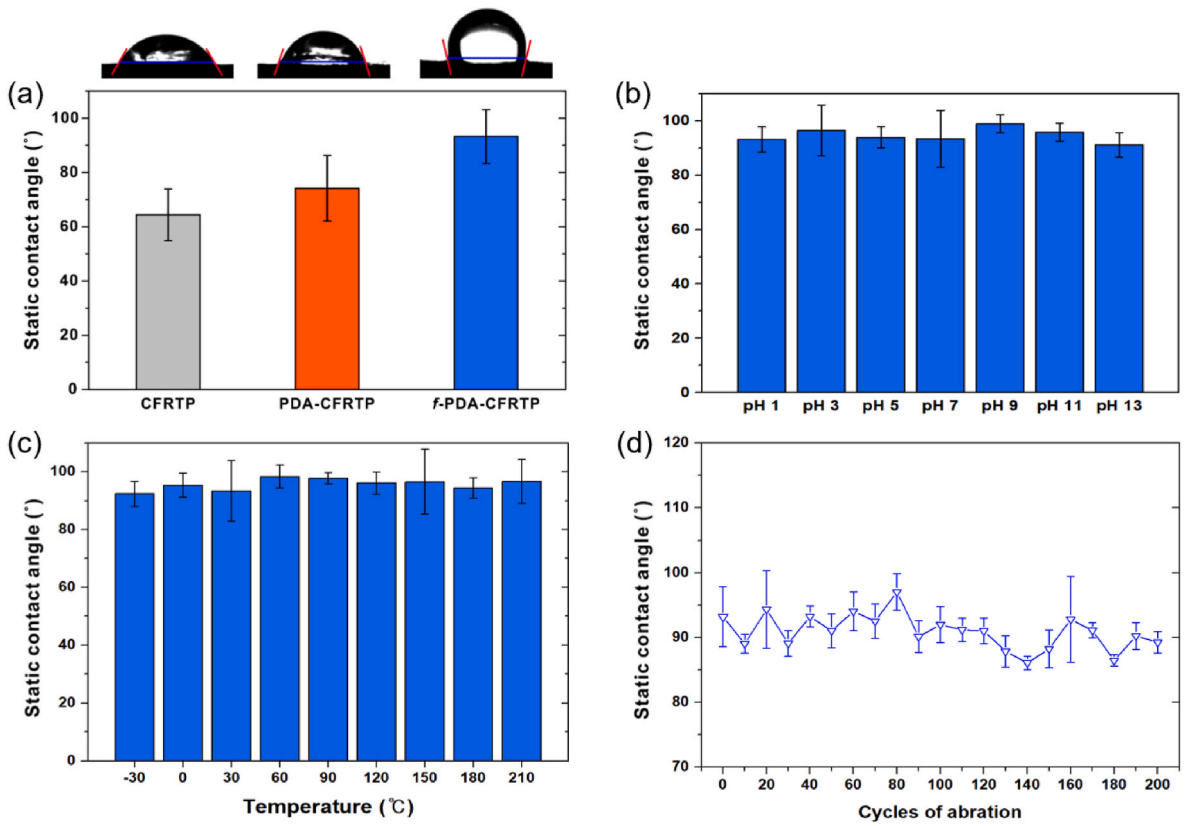

Fig. 5. Static contact angles of (a) CFRTP, PDA-CFRTP, and *f*-PDA-CFRTP with corresponding images of water droplets on the coated surfaces, (b) aqueous solution with different pH on *f*-PDA-CFRTP, (c) *f*-PDA-CFRTP after 30 min of exposure to high/low temperatures, and (d) *f*-PDA-CFRTP after abrasion with 800 grit sandpaper. ($n = 5$).

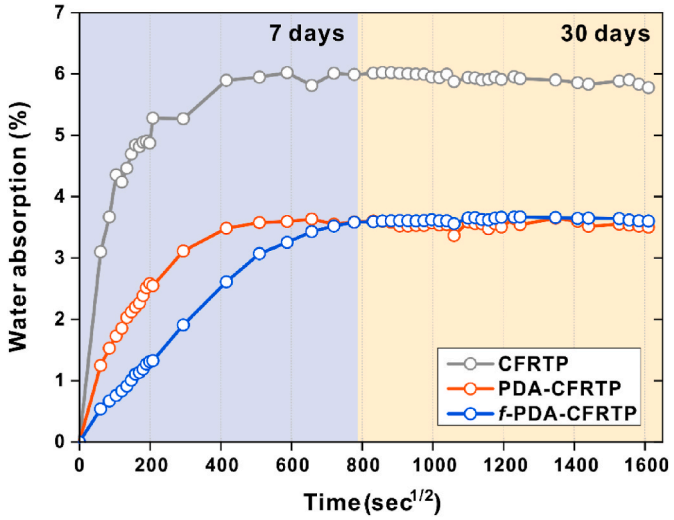

Fig. 6. Water absorption of CFRTP (gray), PDA-CFRTP (red), and *f*-PDA-CFRTP (blue).

absorption at the interface because it represents interfacial bonding. In contrast, flexural strength is affected by the overall water absorption because it represents overall mechanical properties [12].

3.4. Anti-icing test

The anti-icing test of CFRTP and *f*-PDA-CFRTP was conducted to prove the anti-icing performance of *f*-PDA coating (Fig. S6, Fig. 8). As a result of continuously dropping water on the specimens, water adhered to the surface of CFRTP due to the hydrophilic surface and high surface energy of CFRTP to form ice. Depending on the time, the surface area and size of the ice continued to increase. However, on the surface of *f*-FDA-CFRTP, water droplets immediately rolled out of the specimen owing to the effects of hydrophobicity, low surface energy, and the Wenzel or Cassie–Baxter state. This anti-icing performance was effective even after 30 min at −10 °C, and as a result, no ice was accumulated on the surface. The effectiveness of the *f*-PDA coating on the CFRTP was validated through the anti-icing test, and it is expected to aid in applying CFRTP as external parts in various industries.

The Owens–Wendt equation was used to verify the anti-icing performance of the coatings [37,38]. Surface energy was quantified by calculating the Owens–Wendt equation below using the contact angle of water and diiodomethane (Table 1).

$$\gamma_{SL} = \gamma_{SG} + \gamma_{LG} - 2\left(\gamma_{SG}^{d} \bullet \gamma_{LG}^{d}\right)^{1/2} - 2\left(\gamma_{SG}^{p} \bullet \gamma_{LG}^{p}\right)^{1/2}, \quad (3)$$

$$\gamma_{LG}(1+\cos\theta) = 2\left(\gamma_{SG}^{d} \bullet \gamma_{LG}^{d}\right)^{1/2} + 2\left(\gamma_{SG}^{p} \bullet \gamma_{LG}^{p}\right)^{1/2}, \quad (4)$$

$$\gamma_{SG} = \gamma_{SG}^{d} + \gamma_{SG}^{p}, \quad (5)$$

where γ_{SG} is the surface free energy of the solid, γ_{SL} is the interfacial tension between the liquid and solid, γ_{LG} is the surface tension of the liquid, θ is the contact angle, and γ^{d} and γ^{p} are the dispersion and polar components, respectively. Consequently, the surface energy of CFRTP was 47.8 dyne/cm^2, similar to the surface energy of a typical PA 6 of 46 dyne/cm^2. In the case of PDA-CFRTP, the surface energy was 44.4 dyne/cm^2, which was slightly reduced compared to CFRTP. However, in the case of *f*-PDA-CFRTP, the contact angles of water and diiodomethane were significantly increased by 27° and 37°, respectively, and the

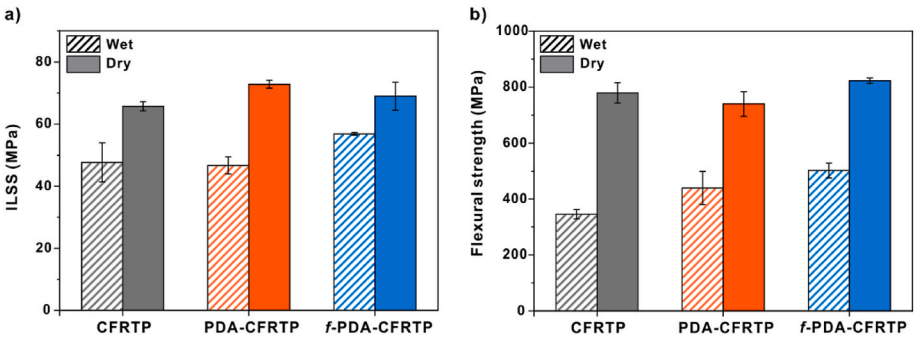

Fig. 7. (a) ILSS and (b) flexural strength of CFRTP, PDA/CFRTP, and *f*-PDA/CFRTP.

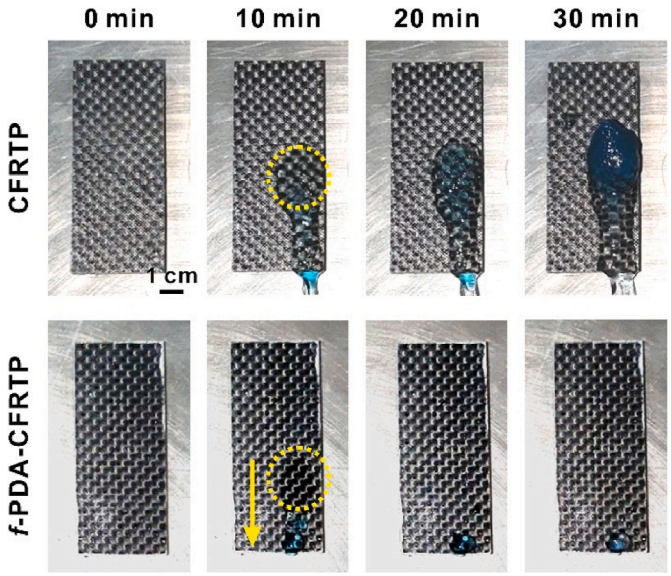

Fig. 8. Images of the anti-icing test specimens of CFRTP and *f*-PDA-CFRTP under exposure to cryogenic chamber at −10 °C over time.

Table 1
Static water and diiodomethane contact angles on CFRTPs and surface free energies of CFRTPs.

Substrates	Contact angles (°)		Surface energies (dyne/cm^2)		
	θ_{water}	$\theta_{diiodomethane}$	γ^D	γ^P	γ
CFRTP	64.4	30.0	37.1	10.7	47.8
PDA-CFRTP	73.2	32.4	38.3	6.1	44.4
f-PDA-CFRTP	90.1	69.6	19.8	4.6	24.4

surface energy was 24.4 dyne/cm^2, which was decreased by 49% compared to the CFRTP. Considering that the surface energies of the representative anti-icing polymers such as PVDF (28 dyne/cm^2) and poly(tetrafluoroethylene) (PTFE) (18 dyne/cm^2) [39], it is concluded that the introduction of *f*-PDA coating significantly reduced the surface energy of PA 6 and thus can offer a new alternative with its superior anti-icing performance. We have focused on two factors affecting the anti-icing performance, one is surface energy as a chemical viewpoint and the other is friction between solid and liquid droplet as a physical viewpoint. Therefore, in our anti-icing test, we intentionally dropped a large amount of water (totally 60 mL) continuously from a height of 10 cm to facilitate water rolling down the surface, instead of conducting a typical contact angle test using a single droplet of water. This experiment is intended to be evaluated under realistic conditions that mimic the actual use of composite materials. The results showed that the low surface energy of *f*-PDA and the reduced friction due to PDA coating synergistically contributed to promote the movement of water droplets in comparison with the pristine CFRTP.

4. Conclusion

This study improved the water resistance of the CFRTP and reduced its surface energy by introducing a sequential surface coating of mussel-inspired PDA coating with fluorinated coating, *f*-PDA, to enable the CFRTP to apply the external components of various industries. Changes in morphology were observed with AFM and SEM, and the effective surface coating was verified using XPS and EDS. Moreover, the hydrophobic *f*-PDA-CFRTP reduced the water absorption by 42%, and, as a consequence, the ILSS and flexural strength of the immersed CFRTP were improved. Furthermore, the surface energy of the *f*-PDA-CFRTP was reduced by 49%, which is similar to that of PVDF and PTFE, significantly improving the anti-icing performance of the resulting composite. We anticipate that *f*-PDA coating can provide a novel platform for applying PA 6-based CFRTP as various external components used in humid environments.

Author statement

Seung Mo Son: Methodology, Investigation, Data Curation, Writing - Original Draft.
Minjung Kim: Methodology, Investigation, Writing - Original Draft.
Jung Jae Yoo: Investigation, Validation.
Min Seong Kim: Investigation, Data Curation.
Byeong-Su Kim: Conceptualization, Writing - Review & Editing, Supervision.
Dong Gi Seong: Conceptualization, Writing - Review & Editing, Supervision, Funding acquisition.

Declaration of competing interest

The authors declare that they have no known competing financial interests or personal relationships that could have appeared to influence the work reported in this paper.

Data availability

Data will be made available on request.

Acknowledgements

This research was supported by the National Research Foundation of Korea (NRF) funded by Ministry of Science and ICT (2022M3H4A1A04076372 and 2021R1A2C3004978).

Appendix A. Supplementary data

Supplementary data to this article can be found online at https://doi.org/10.1016/j.compscitech.2023.110048.

References

[1] R. Shida, K. Tsumuraya, S. Nakatsuka, J. Takahashi, Effect of Automobile Lightning by CFRP on the World Energy Saving, The ninth Japan international SAMPE symposium, 2005, pp. 8–13.

[2] A. Dogan, V. Arikan, Low-velocity impact response of E-glass reinforced thermoset and thermoplastic based sandwich composites, Compos. Part B Eng. 127 (2017) 63–69, https://doi.org/10.1016/j.compositesb.2017.06.027.

[3] R. Stewart, Thermoplastic composites—recyclable and fast to process, Reinforc Plast 55 (3) (2011) 22–28, https://doi.org/10.1016/S0034-3617(11)70073-X.

[4] J.M. Henshaw, W. Han, A.D. Owens, An overview of recycling issues for composite materials, J. Thermoplast. Compos. Mater. 9 (1) (1996) 4–20, https://doi.org/10.1177/089270579600900102.

[5] E. Botelho, M. Rezende, B. Lauke, Mechanical behavior of carbon fiber reinforced polyamide composites, Compos. Sci. Technol. 63 (13) (2003) 1843–1855, https://doi.org/10.1016/S0266-3538(03)00119-2.

[6] T. Ageyeva, I. Sibikin, J. Karger-Kocsis, Polymers and related composites via anionic ring-opening polymerization of lactams: recent developments and future trends, Polymer 10 (4) (2018) 357, https://doi.org/10.3390/polym10040357.

[7] K. Van Rijswijk, S. Lindstedt, D. Vlasveld, H. Bersee, A. Beukers, Reactive processing of anionic polyamide-6 for application in fiber composites: a comparitive study with melt processed polyamides and nanocomposites, Polym. Test. 25 (7) (2006) 873–887, https://doi.org/10.1016/j.polymertesting.2006.05.006.

[8] K. Van Rijswijk, A. Van Geenen, H. Bersee, Textile fiber-reinforced anionic polyamide-6 composites. Part II: Investigation on interfacial bond formation by short beam shear test, Compos. Appl. Sci. Manuf. 40 (8) (2009) 1033–1043, https://doi.org/10.1016/j.compositesa.2009.02.018.

[9] K. Ueda, K. Yamada, M. Nakai, T. Matsuda, M. Hosoda, K. Tai, Synthesis of high molecular weight nylon 6 by anionic polymerization of ε-caprolactam, Polym. J. 28 (5) (1996) 446–451, https://doi.org/10.1295/polymj.28.446.

[10] K. Ueda, M. Nakai, M. Hosoda, K. Tai, Synthesis of high molecular weight nylon 6 by anionic polymerization of ε-caprolactam. Mechanism and kinetics, Polym. J. 29 (7) (1997) 568–573, https://doi.org/10.1295/polymj.29.568.

[11] V. Venoor, J.H. Park, D.O. Kazmer, M.J. Sobkowicz, Understanding the effect of water in polyamides: a review, Polym. Rev. 61 (3) (2021) 598–645, https://doi.org/10.1080/15583724.2020.1855196.

[12] Y. Ma, S. Jin, T. Yokozeki, M. Ueda, Y. Yang, E.A. Elbadry, H. Hamada, T. Sugahara, Effect of hot water on the mechanical performance of unidirectional carbon fiber-reinforced nylon 6 composites, Compos. Sci. Technol. 200 (2020), 108426, https://doi.org/10.1016/j.compscitech.2020.108426.

[13] C.-H. Shen, G.S. Springer, Moisture absorption and desorption of composite materials, J. Compos. Mater. 10 (1) (1976) 2–20, https://doi.org/10.1177/002199837601000101.

[14] H. Schonhorn, F.W. Ryan, Effect of polymer surface morphology on adhesion and adhesive joint strength. II. FEP Teflon and nylon 6, J. Polym. Sci. Polym. Chem. 7 (1) (1969) 105–111, https://doi.org/10.1002/pol.1969.160070108.

[15] T. Muthukumar, A. Aravinthan, K. Lakshmi, R. Venkatesan, L. Vedaprakash, M. Doble, Fouling and stability of polymers and composites in marine environment, Int. Biodeterior. Biodegrad. 65 (2) (2011) 276–284, https://doi.org/10.1016/j.ibiod.2010.11.012.

[16] A. Rosenhahn, S. Schilp, H.J. Kreuzer, M. Grunze, The role of "inert" surface chemistry in marine biofouling prevention, Phys. Chem. Chem. Phys. 12 (17) (2010) 4275–4286, https://doi.org/10.1039/C001968M.

[17] Y. Cao, W. Tan, Z. Wu, Aircraft icing: an ongoing threat to aviation safety, Aero. Sci. Technol. 75 (2018) 353–385, https://doi.org/10.1016/j.ast.2017.12.028.

[18] K. Wei, Y. Yang, H. Zuo, D. Zhong, A review on ice detection technology and ice elimination technology for wind turbine, Wind Energy 23 (3) (2020) 433–457, https://doi.org/10.1002/we.2427.

[19] R. Durai Prabhakaran, Are reactive thermoplastic polymers suitable for future wind turbine composite materials blades? Mech. Adv. Mater. Struct. 21 (3) (2014) 213–221, https://doi.org/10.1080/15376494.2013.834090.

[20] C. Yang, J. Chao, J. Zhang, Z. Zhang, X. Liu, Y. Tian, D. Zhang, F. Chen, Functionalized CFRP surface with water-repellence, self-cleaning and anti-icing properties, Colloids Surf. A Physicochem. Eng. Asp. 586 (2020), 124278, https://doi.org/10.1016/j.colsurfa.2019.124278.

[21] B. Wu, J. Lyu, C. Peng, J. Liu, S. Xing, D. Jiang, S. Ju, M.K. Tiwari, Compression molding processed superhydrophobic CB/CeO2/PVDF/CF nanocomposites with highly robustness, reusability and multifunction, Colloids Surf. A Physicochem. Eng. Asp. 590 (2020), 124533, https://doi.org/10.1016/j.colsurfa.2020.124533.

[22] J.H. Ryu, P.B. Messersmith, H. Lee, Polydopamine surface chemistry: a decade of discovery, ACS Appl. Mater. Interfaces 10 (9) (2018) 7523–7540, https://doi.org/10.1021/acsami.7b19865.

[23] H. Lee, S.M. Dellatore, W.M. Miller, P.B. Messersmith, Mussel-inspired surface chemistry for multifunctional coatings, Science 318 (5849) (2007) 426–430, https://doi.org/10.1126/science.1147241.

[24] E. Shin, C. Lim, U.J. Kang, M. Kim, J. Park, D. Kim, W. Choi, J. Hong, C. Baig, D. W. Lee, Mussel-inspired copolyether loop with superior antifouling behavior, Macromolecules 53 (9) (2020) 3551–3562, https://doi.org/10.1021/acs.macromol.0c00481.

[25] M. Kim, J. Park, K.M. Lee, E. Shin, S. Park, J. Lee, C. Lim, S.K. Kwak, D.W. Lee, B.-S. Kim, Peptidomimetic wet-adhesive PEGtides with synergistic and multimodal hydrogen bonding, J. Am. Chem. Soc. 144 (14) (2022) 6261–6269, https://doi.org/10.1021/jacs.1c11737.

[26] D. Hong, K. Bae, S.-P. Hong, J.H. Park, I.S. Choi, W.K. Cho, Mussel-inspired, perfluorinated polydopamine for self-cleaning coating on various substrates, Chem. Commun. 50 (79) (2014) 11649–11652, https://doi.org/10.1039/C4CC02775B.

[27] H.A. Lee, E. Park, H. Lee, Polydopamine and its derivative surface chemistry in material science: a focused review for studies at KAIST, Adv. Mater. 32 (35) (2020), 1907505, https://doi.org/10.1002/adma.201907505.

[28] Z. Li, X. Zhao, G. Li, F. Gong, Y. Liu, Q. Yan, Z. Yang, F. Nie, Surface fluorination of n-Al particles with improved combustion performance and adjustable reaction kinetics, Chem. Eng. J. 425 (2021), 131619.

[29] N. Sun, B. Zhu, X. Gao, K. Qiao, Y. Zhang, B. Wang, J. Fan, K. Yu, C. Liu, C. Li, Improved the interfacial characteristics of carbon fiber/polyamide 6 composites by synthesizing polydopamine rapidly on the carbon fiber surface with ultrasound-assisted, Compos. Sci. Technol. 234 (2023), 109950.

[30] S.H. Hong, S. Hong, M.H. Ryou, J.W. Choi, S.M. Kang, H. Lee, Sprayable ultrafast polydopamine surface modifications, Adv. Mater. Interfac. 3 (11) (2016), 1500857.

[31] A. Marmur, The lotus effect: superhydrophobicity and metastability, Langmuir 20 (9) (2004) 3517–3519, https://doi.org/10.1021/la036369u.

[32] B. Bhushan, Y.C. Jung, Natural and biomimetic artificial surfaces for superhydrophobicity, self-cleaning, low adhesion, and drag reduction, Prog. Mater. Sci. 56 (1) (2011) 1–108, https://doi.org/10.1016/j.pmatsci.2010.04.003.

[33] Z. Zhao, H. Chen, Y. Zhu, X. Liu, Z. Wang, J. Chen, A robust superhydrophobic anti-icing/de-icing composite coating with electrothermal and auxiliary photothermal performances, Compos. Sci. Technol. 227 (2022), 109578.

[34] S.-H. Lee, J. Kim, M. Seong, S. Kim, H. Jang, H.W. Park, H.E. Jeong, Magneto-responsive photothermal composite cilia for active anti-icing and de-icing, Compos. Sci. Technol. 217 (2022), 109086.

[35] C. El-Mazry, O. Correc, X. Colin, A new kinetic model for predicting polyamide 6-6 hydrolysis and its mechanical embrittlement, Polym. Degrad. Stabil. 97 (6) (2012) 1049–1059, https://doi.org/10.1016/j.polymdegradstab.2012.03.003.

[36] C.R. Davis, Crystallization behavior and mechanical properties of a nylon-6,-6/6, and-12 terpolyamide, J. Appl. Polym. Sci. 62 (13) (1996) 2237–2245, https://doi.org/10.1002/(SICI)1097-4628(19961226)62:13<2237::AID-APP8>3.0.CO;2-K.

[37] D.K. Owens, R. Wendt, Estimation of the surface free energy of polymers, J. Appl. Polym. Sci. 13 (8) (1969) 1741–1747, https://doi.org/10.1002/app.1969.070130815.

[38] D. Janssen, R. De Palma, S. Verlaak, P. Heremans, W. Dehaen, Static solvent contact angle measurements, surface free energy and wettability determination of various self-assembled monolayers on silicon dioxide, Thin Solid Films 515 (4) (2006) 1433–1438, https://doi.org/10.1016/j.tsf.2006.04.006.

[39] S. Dexter, J. Sullivan Jr., J. Williams III, S. Watson, Influence of substrate wettability on the attachment of marine bacteria to various surfaces, Appl. Microbiol. 30 (2) (1975) 298–308, https://doi.org/10.1128/am.30.2.298-308.1975.